International Journal of Bifurcation and Chaos

Paper submitted to the Special Issue of 2010DDays

HYSTERESIS OF PERIODIC AND CHAOTIC PASSIVE Q-SWITCHING SELF-PULSATIONS IN A MOLECULAR LASER MODEL, AND THE STARK EFFECT AS A CODIMENSION-2 PARAMETER.

EUSEBIUS J. DOEDEL
Department of Computer Science and Software Engineering, Concordia University, 1455 boulevard de Maisonneuve O., Montréal, Québec H3G 1M8, Canada
doedel@cse.concordia.ca

CARLOS L. PANDO L.
Instituto de Física, Benemérita Universidad Autónoma de Puebla, Apdo. Postal J-48, Puebla, Pue. 72570, México
carlos@sirio.ifuap.buap.mx

Received (to be inserted by publisher)

We give a systematic comparison of a molecular model for a CO_2 laser with a fast saturable absorber and a reduced version of this model. Overall, we find that there is good agreement between these models. We use numerical continuation algorithms to analyze the bifurcation structure of the equations, and complement the results by numerical simulations to model possible experiments. Our study predicts the existence of isolas of periodic passive Q-switching self-pulsations and a rich structure of Q-intervals of stability for these periodic orbits, where Q represents the incoherent pump of the laser. These intervals correspond to the observed phenomenon known as period-adding cascades. Computed loci of codimension-1 bifurcations show that a small shift of a secondary parameter in the reduced model with respect to that of the complete model substantially improves their quantitative agreement. This parameter is associated with the action of the Stark effect in the absorber. We also discuss a necessary condition for chaotic windows to arise as Q changes: the codimension-1 loci suggest that at most two such chaotic windows typically exist.

Keywords: lasers; bifurcation analysis; numerical continuation; transition to chaos.

1. Introduction

Experimental evidence of low dimensional chaos in lasers is a good example of the correspondence between chaos in a physical system and its theoretical model. Indeed, in the study of laser instabilities, infrared gas lasers remain promising systems as these can realize an almost one-to-one correspondence between experiment and theory, because of their known energy-level structure and parameters [Arecchi, 1987]. In this article we compare a molecular model of a gas laser with a saturable absorber and its reduced version, within the context of codimension-1 and codimension-2 bifurcations. Lasers with an intracavity saturable

absorber (LSA), which generate passive Q-switching (PQS) self-pulsations, have long been used to generate high-intensity laser spikes. As a result, the complex dynamics generated by these giant spikes have been the subject of numerous studies [Mandel, 1997; Abraham *et al.*, 1998; Siegman, 1986; Keller, 2003; Erneux *et al.*, 2010].

The temporal behavior of the CO_2 laser system with a gaseous saturable absorber inside the laser cavity was first observed by Wood and Schwarz [Wood *et al.*, 1967] and later analyzed by many others [Burak *et al.*, 1971; Dupré *et al.*, 1975; Arimondo *et al.*, 1983; Tachikawa *et al.*, 1986, 1987, 1988]. Typically, in a single-mode homogeneously broadened CO_2 LSA, each PQS periodic self-pulsation consists of a leading spike, named the reinjection, and $n-1$ small intensity undulations in a tail [Lefranc *et al.*, 1991; Cavalcante & Rios Leite, 2008]. We label these PQS periodic self-pulsations as $\Pi^{(n)}$. CO_2 LSA are physical systems with a rich dynamical phenomenology and their versatility to change control parameters is a significant advantage for studies in nonlinear dynamics [Erneux *et al.*, 2010; Lefranc *et al.*, 1991; Cavalcante & Rios Leite, 2008; Papoff *et al.*, 1992].

In this article we demonstrate for the case of a molecular CO_2 LSA model that the complete model (CM) and a reduced model (RM), both give rise to isolas of periodic PQS self-pulsations as a suitable parameter, namely the incoherent external pump, is changed. By an *isola*, we mean a smooth and closed one-dimensional family of periodic solutions, as a single control parameter is allowed to vary [Olsen *et al.*, 1999; Doedel, 1984]. These periodic solutions, stable or unstable, are precisely the aforementioned $\Pi^{(n)}$. We believe that these isolas may be found experimentally using control techniques in dynamical systems [Boccaletti *et al.*, 2000; Sieber *et al.*, 2008]. The latter may foster further studies of the accessible experimental dynamics of the CO_2 LSA.

Following a reduction procedure, which has been successfully applied before to reduce the number of effective equations in CO_2 lasers [Ciofini *et al.*, 1993; Braza, 1999], we obtained the RM from the CM [Doedel *et al.*, 2011a]. Moreover, this procedure, known as the *reduction principle*, is quite generally applicable, as suggested in [Kuznetsov, 2004].

Diagrams showing Poincaré section simulations of the CM and the RM, as the incoherent pump parameter is varied, show some differences; in particular new windows of chaotic behavior. Nevertheless, bifurcation diagrams obtained by numerical continuation [Doedel *et al.*, 2011], are to a significant extent qualitatively the same. We will explain how these divergences arise and how to improve the quality of the agreement between both the CM and RM.

As the pump parameter is changed in an experiment, period-adding cascades of PQS periodic self-pulsations arise: $\Pi^{(n)} \rightarrow \Pi^{(n+1)}$ or vice versa [Lefranc *et al.*, 1991; Cavalcante & Rios Leite, 2008; Hennequin *et al.*, 1998; Dangoisse *et al.*, 1988; Tohei *et al.*, 1992]. According to the CM and RM, the origin of the period-adding cascades stems from the coexistence of stable $\Pi^{(n)}$ along different isolas.

In a widely used CO_2 LSA model known as the 3-2 level model [Tachikawa *et al.*, 1986, 1987, 1988; Lefranc *et al.*, 1991; Cavalcante & Rios Leite, 2008], it was found that the simulated time series is consistent with the experimental chaotic time series obtained from the CO_2 LSA [Papoff *et al.*, 1992]. In a recent study of the 3-2 level model we showed that the aforementioned isola structures exist [Doedel *et al.*, 2011b]. However, details of the bifurcations along the isolas in that model qualitatively differ from those reported for the CM and the RM in this paper. As for the physics, the 3-2 level model is a generalization of the two-level rate-equation model of the LSA, suitably modified to take into account the presence of a third level in the amplifier, where only the most relevant relaxation mechanisms have been included. Although the 3-2 level model neglects the effects of inhomogeneous broadening, it provides surprisingly good agreement with experimental observations. This contrasts with an earlier version of the four-level model for the the CO_2 LSA [Arimondo *et al.*, 1983], which did not predict the PQS $\Pi^{(n)}$ observed experimentally [Tachikawa *et al.*, 1987, 1988; Lefranc *et al.*, 1991]. The equations in [Arimondo *et al.*, 1983] are based on the dual four-level model, both in the amplifier and in the absorber. In the CM, however, we assume that the amplifier and the absorber are described by a four-level model and a two-level model, respectively [Pando, 1996]. As a result, the CM is able to reproduce the basic operating regimes of the CO_2 LSA, in particular the PQS pulses for different $\Pi^{(n)}$, as the pump parameter is varied. In contrast to the 3-2 level model, however, the CM and the RM depend explicitly on the number of rotational levels in the amplifier. This dependence has physical relevance [Meucci *et al.*, 1992; Zehnle *et al.*, 1992; Pando *et al.*, 1993]. In early studies of the

CO_2 LSA using the 3-2 level model, it was pointed out that the physical mechanism of the undamped $n-1$ undulations of $\Pi^{(n)}$ is related to relaxation oscillations caused in the balance between the induced emission and the relaxation of the lower laser level in the amplifier [Tachikawa *et al.*, 1986]. These are precisely the kind of oscillations that switch between fast and slow motions and small and large amplitudes, and which arise in a large family of physical systems. They are now known as mixed mode oscillations [Brons *et al.*, 2008], and the CO_2 LSA is a good example thereof.

Another issue that has been considered experimentally and in simulations is the frequency locking phenomenon induced by the *Stark effect*, where a periodically modulated external electrical field acts upon the absorber cell [Dangoisse *et al.*, 1990; Tsukamoto *et al.*, 1995]. In this context we also consider the bifurcations of the periodic PQS self-pulsations induced by a constant (DC) electrical field, which acts as a second bifurcation parameter.

This article is organized as follows. In Sec. 2 we discuss the CM of the CO_2 laser with a fast saturable absorber (LSA) and its reduced version (RM). In Sec. 3 we present and compare the basic bifurcation diagrams of these models for variable Q, the incoherent pump, namely, the bifurcation diagrams for the stationary states and those of the main periodic self-pulsation $\Pi^{(1)}$. In Sec. 4, we compare the isola families of periodic self-pulsations $\Pi^{(n)}$, with $n \geq 3$, in the two models, as the parameter Q is varied. In Sec. 5, we consider the changes that the Stark effect, acting upon the absorber cell, induces in the isolas. In particular, we compare how the stability intervals along the isolas in the two models change. Section 6 contains our conclusions.

2. The Model

In contrast to standard laser models, in which a single mode interacts with a resonant molecular transition, in CO_2 lasers the population transfers are more complicated in the amplifier cell and need a four-level system to be modeled [Burak *et al.*, 1971; Dupré *et al.*, 1975; Zambon *et al.*, 1989; Zambon, 1991; Meucci *et al.*, 1992; Zehnle *et al.*, 1992; Pando *et al.*, 1993, 1995]. Taking into account this peculiarity, a model for a LSA considered in [Pando, 1996] accurately simulates the PQS pulses for different $\Pi^{(n)}$ as the pump parameter is varied.

Within the laser cavity the two cells of resonant molecules corresponding to the amplifier and the absorber are described in our LSA model by a four-level model and a two-level model, respectively [Pando, 1996]. Here it is assumed that the lasing atomic transitions are homogeneously broadened. The amplifier equations have the same parameters as those used in the studies of the CO_2 laser with modulated losses [Pando *et al.*, 1993, 1995] and in those dealing with the transient regimes [Meucci *et al.*, 1992; Zehnle *et al.*, 1992]. In both situations good quantitative agreement between models and experiments was found. The saturable absorber, instead, is described by a two-level model, as suggested by several theoretical and experimental studies [Tachikawa *et al.*, 1988; Lefranc *et al.*, 1991; Tohei *et al.*, 1992]. In this article, we consider the case of a fast saturable absorber. It is this cell of absorbing molecules that is affected by the action of a constant external electrical field, namely, the Stark effect [Dangoisse *et al.*, 1990; Tsukamoto *et al.*, 1995], as will be discussed in Sec. 5.

The model is based on the usual field-matter equations in a resonant cavity [Abraham *et al.*, 1998]. With the aforementioned considerations, at exact resonance between the cavity and molecular frequencies, the coupled field-matter rate equations for a single longitudinal mode CO_2 LSA are described by the following set of equations:

$$\frac{dI}{dt} = -KI + \frac{B_g l_g}{L} I(N_2 - N_1) - \frac{B_a l_a}{L} I N_a \ ,$$

$$\frac{dN_2}{dt} = -B_g I(N_2 - N_1) - \gamma_2 N_2 - \gamma_R N_2 + \gamma_R^{'} M_2 + \gamma_2 Q \ ,$$

$$\frac{dN_1}{dt} = B_g I(N_2 - N_1) - \gamma_1 N_1 - \gamma_R N_1 + \gamma_R^{'} M_1 \ ,$$

$$\frac{dM_2}{dt} = -\gamma_2 M_2 + \gamma_R N_2 - \gamma_R^{'} M_2 + \gamma_2 z Q \ ,$$

$$\frac{dM_1}{dt} = -\gamma_1 M_1 + \gamma_R N_1 - \gamma_R^{'} M_1 \ ,$$

$$\frac{dN_a}{dt} = -2B_a I N_a - r(N_a - N_a^*) \ . \qquad (1)$$

Here I stands for the field intensity within the laser cavity. N_2 (M_2) and N_1 (M_1) denote the populations of the upper and lower resonant (nonresonant) rotational energy levels in the gain medium, respectively. N_a is the difference of populations between the lower and upper level in the absorber, which will remain positive. B_g and B_a are the cross sections multiplied by the velocity of light for the induced emission in the gain medium and in the absorber, respectively. Q is the incoherent pump induced by the excitation current in the gain medium. N^* denotes the thermal equilibrium value of N_a, and l_g and L stand for the length of the gain medium and laser cavity, respectively. Furthermore, l_a denotes the length of the absorption cell, K is the cavity loss rate, and z is the effective number of nonlasing rotational levels in each vibrational band. Also, $\gamma_R^{'}$ is the rotational relaxation rate for the transitions between $M_2 \to N_2$ and $M_1 \to N_1$, and γ_R is the rotational relaxation rate for the inverse transitions, $\gamma_R/\gamma_R^{'} = z$. The vibrational relaxation rates for N_1 and N_2 are denoted, respectively, by γ_1 and γ_2. These relaxation rates hold as well for M_1 and M_2, respectively. The relaxation parameter of N_a is given by r.

After normalization of the variables and parameters in Eq. (1), and the adiabatic elimination of N_a, we get the following set of equations, which define the CM:

$$\frac{dI}{dt} = -I + I(N_2 - N_1) - \frac{\alpha I}{1 + 2\beta_r I} \ ,$$

$$\frac{dN_2}{dt} = -I(N_2 - N_1) - \gamma_2 N_2 - \gamma_R N_2 + \gamma_R^{'} M_2 + \gamma_2 Q \ ,$$

$$\frac{dN_1}{dt} = I(N_2 - N_1) - \gamma_1 N_1 - \gamma_R N_1 + \gamma_R^{'} M_1 \ ,$$

$$\frac{dM_2}{dt} = -\gamma_2 M_2 + \gamma_R N_2 - \gamma_R^{'} M_2 + \gamma_2 z Q \ ,$$

$$\frac{dM_1}{dt} = -\gamma_1 M_1 + \gamma_R N_1 - \gamma_R^{'} M_1 \ . \qquad (2)$$

Here I stands for the intensity, which has been normalized by $I \to IB_g/K$. The populations and the pump variable Q in the gain medium have been rescaled identically, *e.g.*, $Q \to QB_g l_g/KL$. The populations N_a and N_a^* in the absorber have been normalized in the same way, *e.g.*, $N_a \to N_a B_g l_g/KL$. All relaxation parameters have been renormalized in the same manner, *e.g.*, $\gamma_1 \to \gamma_1/K$. Time has been rescaled as $t \to t/K$. The parameters α and β_r are defined as

$$\alpha = \frac{B_a l_a N_a^*}{B_g l_g} \ , \qquad \beta_r = \frac{B_a}{B_g r} \ ,$$

where β_r is known as the saturation parameter. The parameter values are $\gamma_1 = 0.08\mu/K$, $\gamma_2 = 0.01\mu/K$, $\gamma_R = z\gamma_R^{'}$, $\gamma_R^{'} = 0.7\mu/K$, $z = 10$, $K = 3.2\mu$, and $\mu = 10^6 \text{sec}^{-1}$ [Pando, 1996; Doedel *et al.*, 2011a]. In this section, as well as in the next section, the control parameter is taken to be Q, while α and β_r remain constant ($\alpha = 0.75$ and $\beta_r = 200$).

The RM is obtained from Eq. 2 by first making a linear transformation to new coordinates. The old coordinates are the energy level populations in the amplifier [Doedel *et al.*, 2011a]. As the relaxation rates of two of these new variables are very large compared to those of the other two, we neglect their time derivatives. The aforementioned linear transformation is related to the eigenvectors of the trivial solution in Eq. 2, where $I = 0$. As a result of this transformation the following equations are obtained:

$$\begin{aligned} \frac{dI}{dt} &= I\left(-1 + \frac{(z+1)\Omega}{z}(w-v) - \frac{\alpha}{1+2\beta_r I}\right) , \\ \frac{dv}{dt} &= \Omega I(w-v) - \gamma_1 v , \\ \frac{dw}{dt} &= \Omega I(v-w) - \gamma_2 w + z\gamma_2 Q , \end{aligned} \tag{3}$$

where

$$\Omega = \frac{z+1}{(z+1)^2 + 2zI/\gamma_R{'}} \quad , \quad v = \frac{zN_1 + zM_1}{z+1} \quad , \quad w = \frac{zN_2 + zM_2}{z+1} .$$

It is worthwhile to point out that the parameter value $z = 10$ for the amplifier has been suggested already in the early studies of the LSA [Arimondo *et al.*, 1983]. Later, the value $z = 10$ has been used in the CO_2 laser within the context of the transient regime [Meucci *et al.*, 1992; Zehnle *et al.*, 1992], the CO_2 laser with modulated losses [Pando *et al.*, 1993] and the CO_2 laser with feedback [Varone *et al.*, 1995]. More recently, a comparison between the 4LM and the six-temperature model for the mechanical Q-switched CO_2 laser was carried out, obtaining typically a good correspondence between experiment and the predictions of both models [Wang *et al.*, 2006]. However, Horlbelt and collaborators [Horbelt *et al.*, 2001] suggested a dependence of the parameters γ_R and $\gamma_R^{'}$ on Q, over a wide interval of the excitation current (Q) in a Q-switched CO2 laser, *i.e.*, from 4.20 mA to 5.20 mA. That is, Q changes about 25 percent above the first laser threshold. As a consequence the parameter z depends also on Q, as z is defined as the ratio of γ_R to $\gamma_R^{'}$. However, the width over which Q induces relevant changes in the CO_2 LSA (as in Fig. 8) is much smaller than that studied in [Horbelt *et al.*, 2001]: just 4 per cent above the relevant value of Q, where z is not expected to change in a relevant way.

3. The Hopf Bifurcation

In both the CM and the RM the trivial solution, for which $I = 0$, is stable when $Q < 1+\alpha$. It loses stability at $Q = 1+\alpha$ due to a transcritical bifurcation, where the trivial solution family and a nonzero steady state solution family intersect. Thus, for $\alpha = 0.75$, the trivial solution loses stability at $Q = 1.75$. For both LSA models, one leg of the bifurcating family of nontrivial stationary solutions consists of unstable solutions until a Hopf bifurcation is reached near $Q = 2.27$, beyond which these equilibria become stable, as shown in Fig. 1a for the CM and in Fig. 1b for the RM.

The numerical computations, carried out with AUTO [Doedel *et al.*, 2011], sensitively depend on how small I gets. For this reason it is better to use a new variable c, where $I = \exp(c)$. The trivial solution, $I = 0$, then corresponds to $c = -\infty$. Note that due to the above transformation the trivial solution cannot be seen in the bifurcation diagrams. Our bifurcation diagrams show the customary L_2-norm versus Q ; for the case of the CM this norm is defined as $(c^2 + N_1^2 + N_2^2 + M_1^2 + M_2^2)^{1/2}$ for the nontrivial stationary solutions, while for periodic solutions of period T we use $\left(\int_0^T [c(t)^2 + N_1(t)^2 + N_2(t)^2 + M_1(t)^2 + M_2(t)^2]\, dt\right)^{1/2}/\sqrt{T}$. Similar expressions define the L_2-norm for the RM.

We note that by its nature a bifurcation diagram shows a representative measure of the solution versus the value of the parameter that is being varied. The choice of the solution measure is mostly dictated by the clarity of the diagram it produces. As such the L_2-norm is a customary measure, as it relects changes

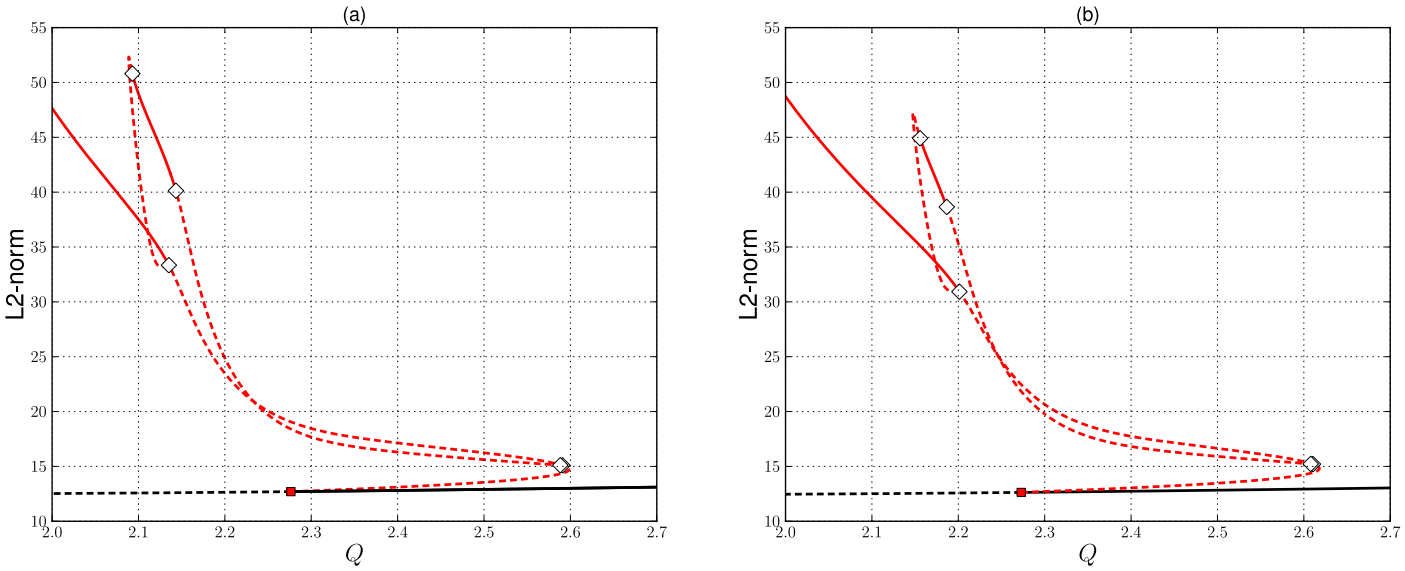

Fig. 1. The bifurcation diagram including the nontrivial stationary solution family (black), the family of 1-pulse periodic orbits (red) that emanates from the Hopf bifurcation (red square), and a period-doubled family of 2-pulse orbits (red) $\Pi^{(2)}$, which connects the two period-doubling bifurcations (open diamonds) on the 1-pulse family. The 2-pulse family contains a region of stability, bordered by secondary period-doubling bifurcations (open diamonds). Solid curves represent stable solutions, and dashed curves represent unstable solutions. Panel (a) is for the CM, and panel (b) is for the RM.

in any of the solution components. For further clarity we also include some bifurcation diagrams that show the period of the orbits versus the varying parameter.

Another representation is to measure the variable c ($I = \exp(c)$, where I is the intracavity laser field intensity), and embed its continuous time dependence in a suitable phase space of delayed coordinates. Here 3 dimensions would be sufficient, as the system is highly dissipative. One can then calculate the relevant norm in terms of these delayed coordinates as a function of the free parameter. The embedding theorem asserts that under suitable conditions the embedded trajectory and that of the original model are topologically equivalent [Kantz, 2004].

We also note that unstable periodic orbits that appear in the bifurcation diagrams are physically relevant, as they may be stabilized when a suitable control mechanism is applied, such as in [Boccaletti *et al.*, 2000; Sieber *et al.*, 2008].

4. Hysteresis of Periodic and Chaotic PQS self-pulsations.

To better appreciate the small differences between the predictions of the CM and the RM, we have done numerical simulations where the pump parameter, Q, is decreased within a suitable interval. Bifurcation diagrams, generated using AUTO [Doedel *et al.*, 2011], then help understand how these differences arise.

To this end, we first integrate both models and, after an appropriate transient time, we plot Q versus c ($I = \exp(c)$) in the Poincaré section, which we define as the surface generated when the maximum of c occurs. The results are shown in Fig. 2a and Fig. 2b for the CM and the RM, respectively. Here, as Q is decreased, a sequential transition $\Pi^{(n+1)} \to \Pi^{(n)}$ is clearly visible, with occasional small windows of chaotic behavior.

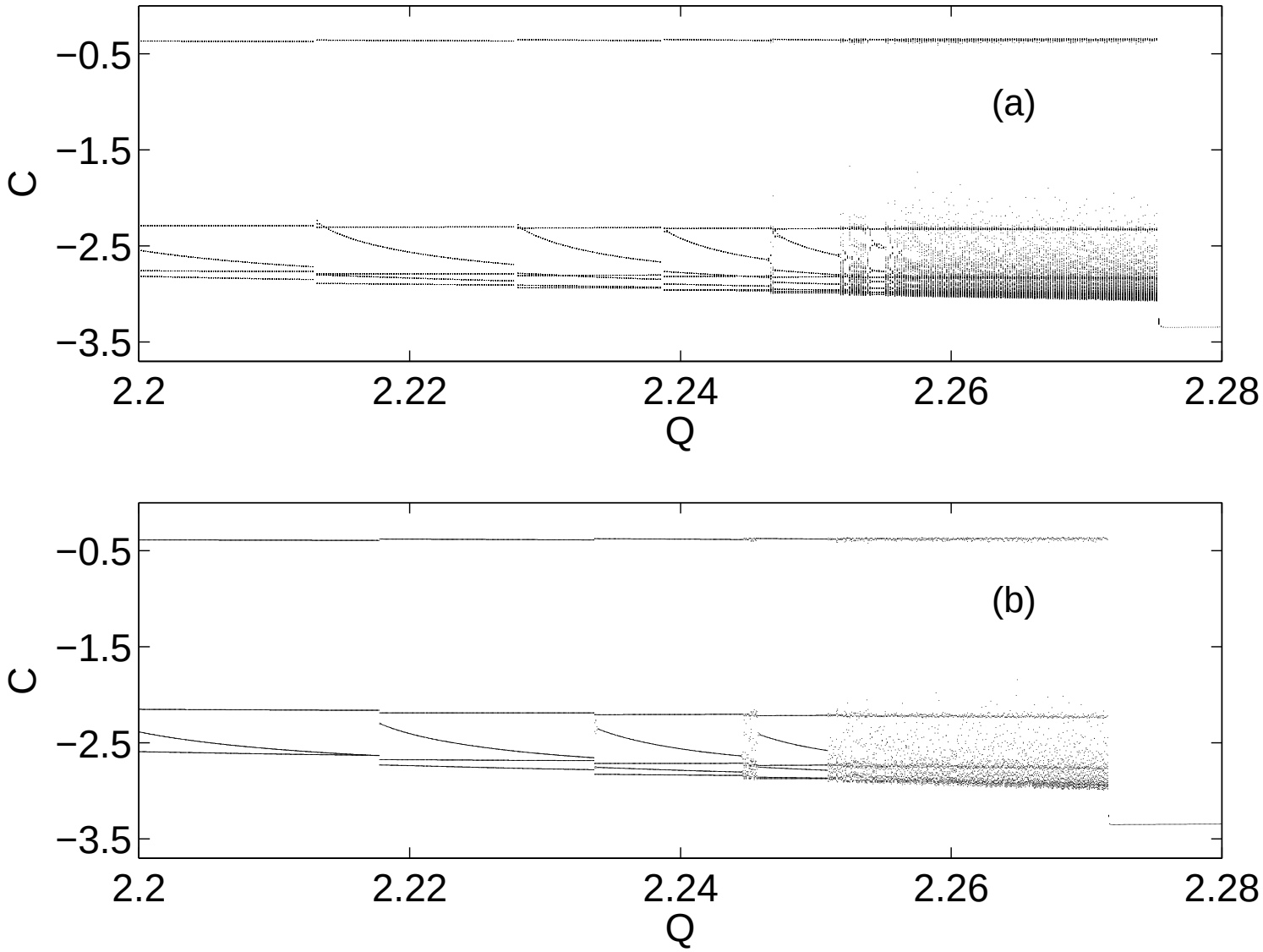

Fig. 2. Plot of c versus Q taken from the Poincaré section, where $\alpha = 0.75$, $\beta_r = 200$, and Q is being decreased. Evident are the period-adding cascades of periodic PQS pulses $\Pi^{(n)}$, and windows of chaotic motion. The Hopf bifurcation occurs at $Q \approx 2.27$, just to the right of where the chaotic motion ceases. Panel (a) is for the CM, and panel (b) is for the RM. We define the Poincaré section as the surface generated when the maxima of c occur.

The periodic time evolution of the stable PQS self-pulsations $\Pi^{(n)}$ is shown for the CM in Fig. 3, for $n = 3, 4, 5, 6$, each of which corresponds to a different value of Q. Similarly, Fig. 4 shows PQS self-pulsations for the RM. This also allows us to identify the corresponding periodic orbits $\Pi^{(n)}$ in Fig. 2a and Fig. 2b, in view of the period-adding cascade property. These PQS self-pulsations correspond qualitatively to those reported in previous studies [Arimondo *et al.*, 1983; Tachikawa *et al.*, 1987, 1988; Lefranc *et al.*, 1991; Cavalcante & Rios Leite, 2008].

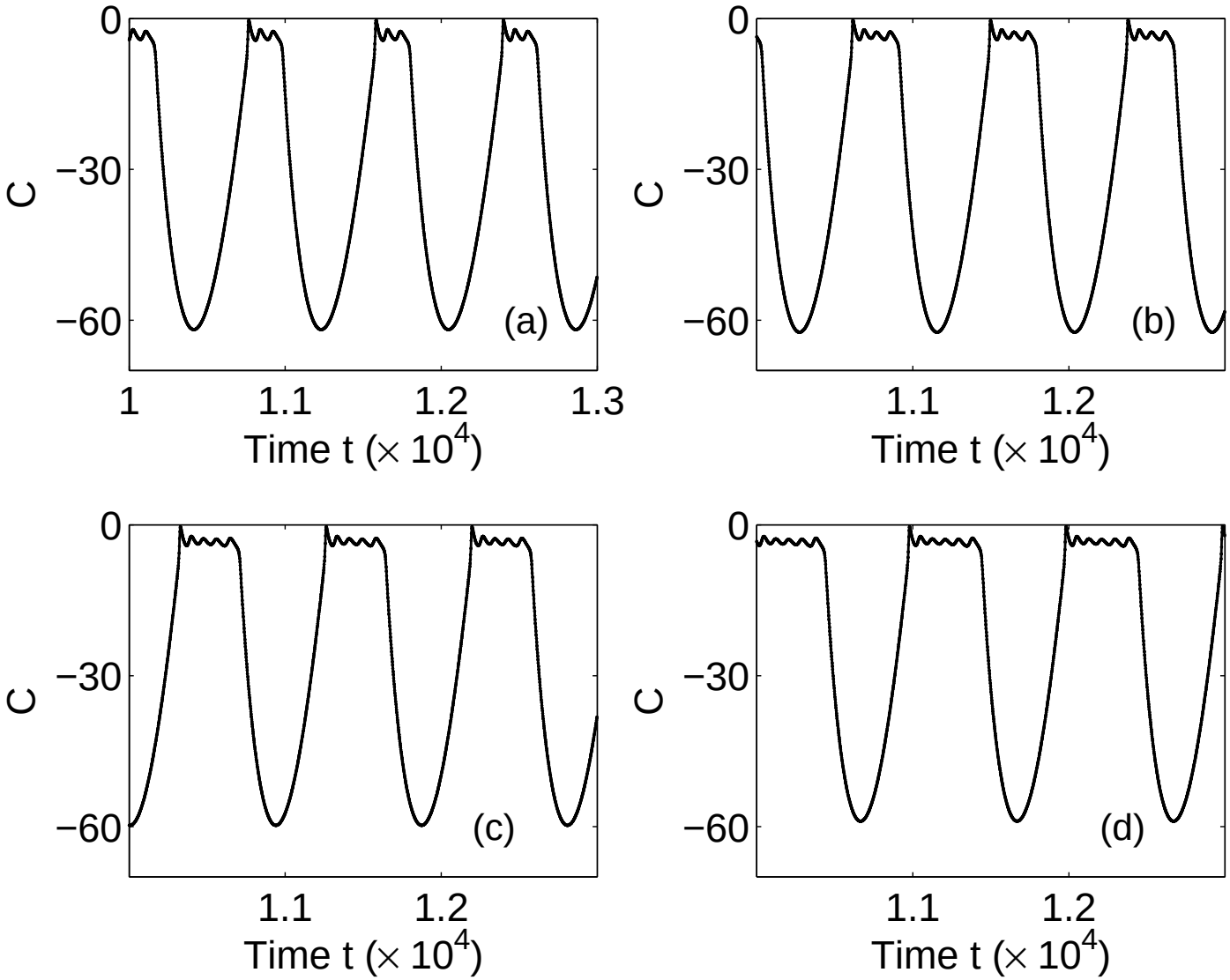

Fig. 3. Plot of c versus time t for the CM, where $\alpha = 0.75$, $\beta_r = 200$, for the stable PQS pulses $\Pi^{(n)}$, $n = 3, 4, 5, 6$. The large negative value of c, down to -60, corresponds to a very small value of I, where $I = e^c$. (a) $\Pi^{(3)}$ for $Q = 2.160$. (b) $\Pi^{(4)}$ for $Q = 2.185$. (c) $\Pi^{(5)}$ for $Q = 2.210$. (d) $\Pi^{(6)}$ for $Q = 2.225$. For each stable PQS pulse $\Pi^{(n)}$ we can see the reinjection (leading spike) and $n - 1$ undulations (undamped relaxations).

Fig. 2a and Fig. 2b suggest that the Hopf bifurcation occurs in the RM for a slighly smaller value of Q than in the CM. This can be seen just before the onset of chaotic behavior, near $Q = 2.27$, when the system is in its stable equilibrium state in both models. Fig. 1a and Fig. 1b show that indeed this is the case, with $Q_{HB}^{(RM)} = 2.2727$ for the RM, and $Q_{HB}^{(CM)} = 2.2765$ for the CM.

The bifurcation diagrams displayed in Fig. 1a for the CM and in Fig. 1b for the RM, also show the family of periodic solutions that emanates from the Hopf bifurcation. In each model, this family contains a fold as well as two period-doubling bifurcations, of which one is near the fold. The periodic solutions are stable beyond the second period-doubling bifurcation. Fig. 1a and Fig. 1b also show that the two period-doubling bifurcations are connected by a single period-doubled family, which contains a region of stability that is bordered by secondary period-doubling bifurcations. These secondary period-doubling bifurcations can lead to more complicated stable dynamics that is, however, confined to very small regions in parameter space. Note that $\Pi^{(2)}$ in Fig. 2a and Fig. 2b corresponds to the period-doubled orbit which emanates from

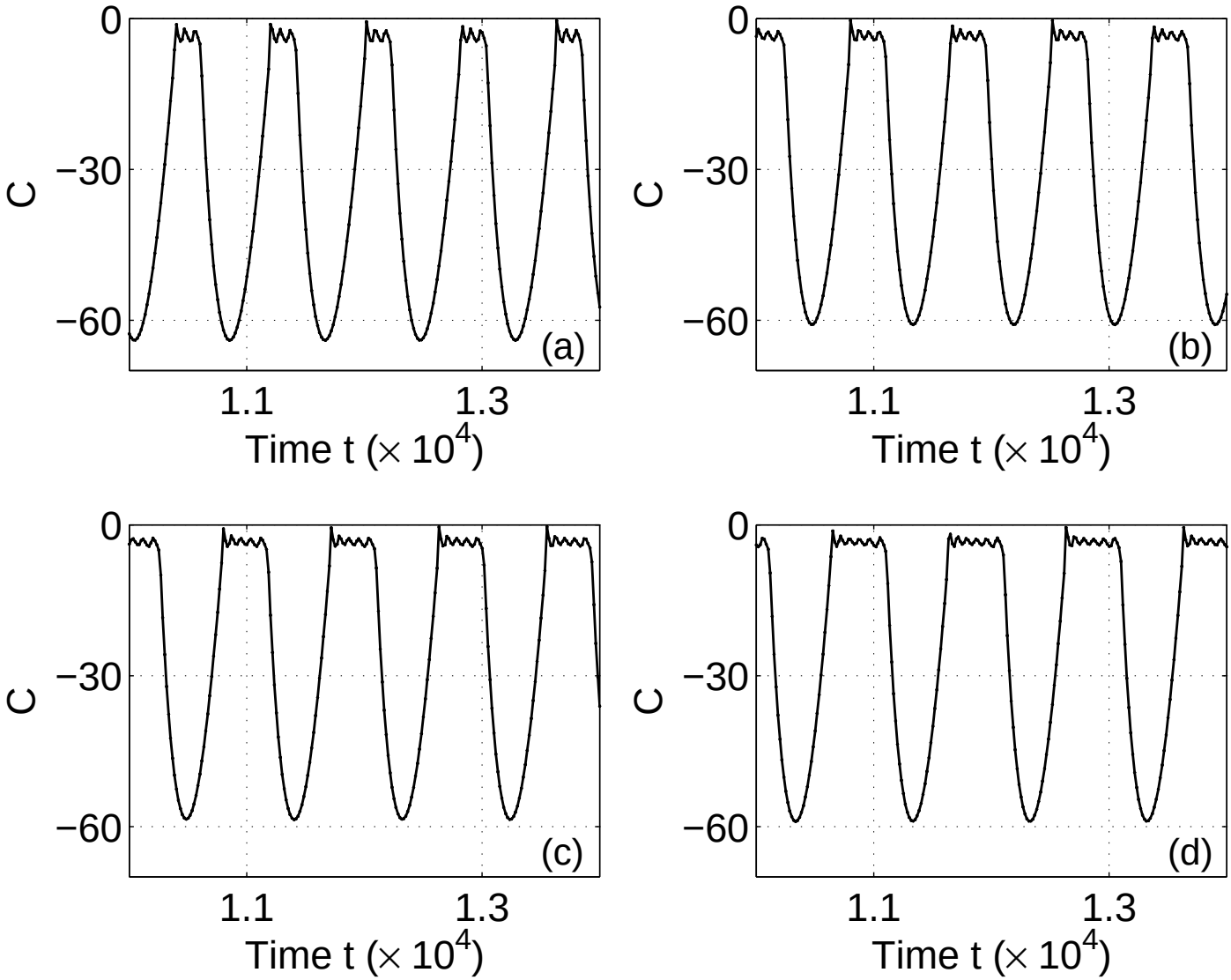

Fig. 4. Plot of c versus time t for the RM, where $\alpha = 0.75$, $\beta_r = 200$, for the stable PQS pulses $\Pi^{(n)}$, $n = 3, 4, 5, 6$. (a) $\Pi^{(3)}$ for $Q = 2.18$. (b) $\Pi^{(4)}$ for $Q = 2.21$. (c) $\Pi^{(5)}$ for $Q = 2.230$. (d) $\Pi^{(6)}$ for $Q = 2.24$. For each stable PQS pulse $\Pi^{(n)}$ we can see the reinjection (leading spike) and $n - 1$ undulations (undamped relaxations).

the main PQS self-pulsation $\Pi^{(1)}$ in Fig. 1a and Fig. 1b, respectively.

Fig. 5a and Fig. 5b, for the CM and the RM, respectively, show that there are additional periodic solution families that cannot be reached directly by periodic solution bifurcations from the families shown in Fig. 1a and Fig. 1b, at least not by only varying the parameter Q. Fig. 5a and Fig. 5b show a number of isolated families (*isolas*) of periodic solutions. We shall refer to these isolas as $\mathcal{I}_n$, $n = 3, 4, 5, 6, \cdots$. The PQS self-pulsation $\Pi^{(n)}$ then belongs to the isola $\mathcal{I}_n$, $n = 3, 4, 5, 6, \cdots$. Moreover, Fig. 5a and Fig. 5b show that each isola $\mathcal{I}_n$ contains fold and period-doubling bifurcations. For each of the isolas shown, the periodic solutions $\Pi^{(n)}$ are stable in a Q-interval bounded by period-doubling bifurcations.

On the basis of Fig. 5a and Fig. 5b one can explain the different types of hysteresis observed in Fig. 2a and Fig. 2b at different values of Q. In enlarged views of the regions of stability in Fig. 5a and Fig. 5b, as shown in Fig. 6, we can clearly see that stable periodic solutions $\Pi^{(n)}$ coexist. In Fig. 6 note, for example, the co-existence of stability regions along the primary periodic family, the period-doubled family, and along the isola $\mathcal{I}_3$; the cause of the hysteresis behavior observed in the simulations.

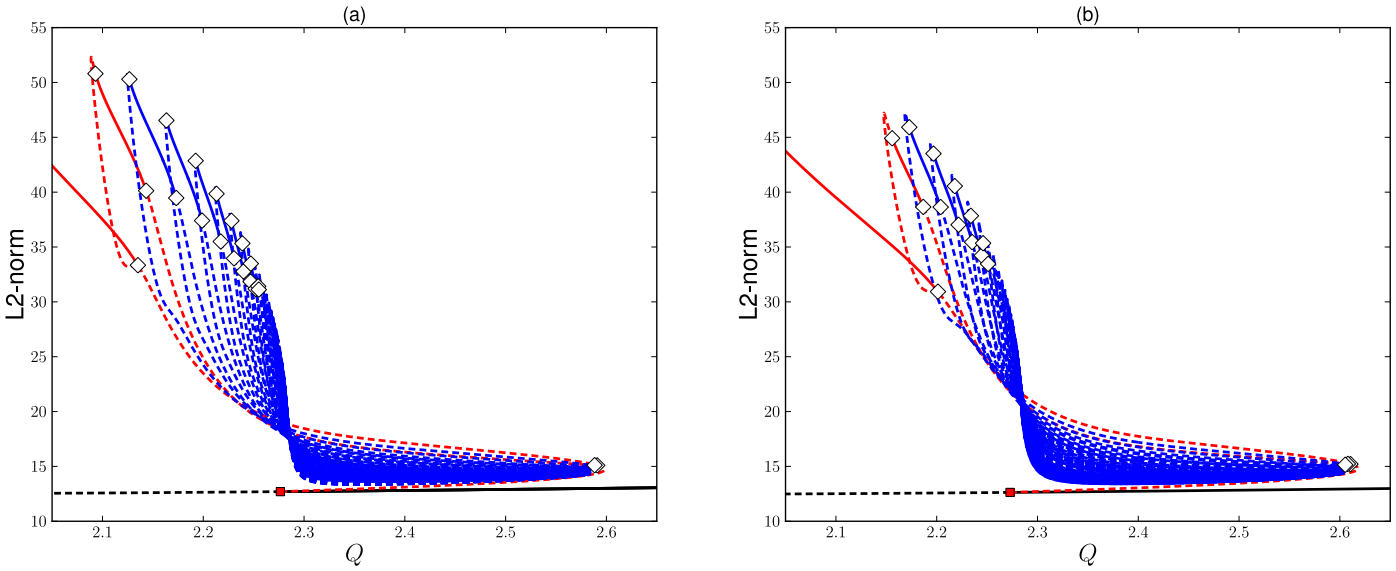

Fig. 5. The bifurcation diagram including the stationary solution family (black) with Hopf bifurcation (the red square), the 1-pulse family (red) from which the period-doubled 2-pulse family (red) arises, and the isolas $\mathcal{I}_n$ for $n = 3, 4, 5, 6, \cdots$ (blue). The stable regions (solid curves) are bordered by period-doubling bifurcations, denoted by open diamonds. Panel (a) is for the CM, and panel (b) is for the RM. A close-up view of the left-hand fold of the isolas and of the period-doublings along the isolas is shown in Fig. 6a and Fig. 6b.

As another example, consider the cascade $\Pi^{(6)} \to \Pi^{(5)}$ observed in both models in Fig. 2a and Fig. 2b. Fig. 2b shows that hysteresis occurs near $Q = 2.234$. This value coincides with that of the leftmost period-doubling (PD) bifurcation along the Q-stability interval for $\Pi^{(6)}$ in Fig. 6b, for which a precise value of Q is 2.23390. Instead, for the CM, Fig. 2a shows that this cascade takes place near $Q = 2.213$. Again, this value coincides with that of the corresponding PD bifurcation along the Q-stability interval for $\Pi^{(6)}$ in Fig. 6a, for which the precise value is given by $Q = 2.21316$. Similarly for the other hysteresis points the associated PD bifurcations for the RM are located to the right of those for the CM.

There are, however, qualitative differences between the hysteresis behavior of the CM and the RM. Consider the cascade $\Pi^{(7)} \to \Pi^{(6)}$ in the CM. Fig. 2a shows that this hysteresis occurs near $Q = 2.228$. This value coincides with that of the leftmost PD bifurcation that borders the Q-stability interval for $\Pi^{(7)}$ in Fig. 6a. The precise value of this PD is $Q = 2.22795$. By contrast, in Fig. 2b near $Q = 2.245$, a window of chaotic behavior (CW) appears in the hysteresis transition: $\Pi^{(7)} \to CW \to \Pi^{(6)}$. (More precisely, by CW we mean that the trajectory is mostly chaotic within a Q-interval in Fig. 2, while it remains possible that there are comparatively smaller windows of periodic behavior.) Correspondingly, the bifurcation diagram for the RM in Fig. 6b shows a gap in Q-values near $Q = 2.245$, where none of the $\Pi^{(n)}$ are stable. Specifically, the leftmost PD bifurcation at $Q = 2.24604$ along the Q-stability interval for $\Pi^{(7)}$ is located to the right of the rightmost PD bifurcation for $\Pi^{(6)}$, at $Q = 2.24466$. These PD bifurcation values for Q are very close to those that bound the CW.

Another feature that can be observed in Fig. 2b and Fig. 6b is that very close to the rightmost PD bifurcation for $\Pi^{(7)}$ along the Q-stability interval, the RM predicts chaotic behavior starting from $Q = Q_{ch} \approx 2.251$ until $Q = Q_{HB}^{(RM)} = 2.27274$. The Q-value for this PD bifurcation is $Q = 2.25101$. Indeed, as Q is decreased from values where the nontrivial stationary solution is stable, the solution of the RM becomes chaotic as soon as Q passes the Hopf bifurcation value. As Q is decreased further, the solution remains mostly chaotic, that is, we have a CW until the value $Q = Q_{ch}$ is reached, as seen in Fig. 2b. Note that the Q-interval between the Hopf bifurcation and the rightmost PD bifurcation of the Q-stability interval for $\Pi^{(7)}$ is a gap, where none of the $\Pi^{(n)}$ are stable. Again, this PD bifurcation value for Q is very close to the left bound of the CW.

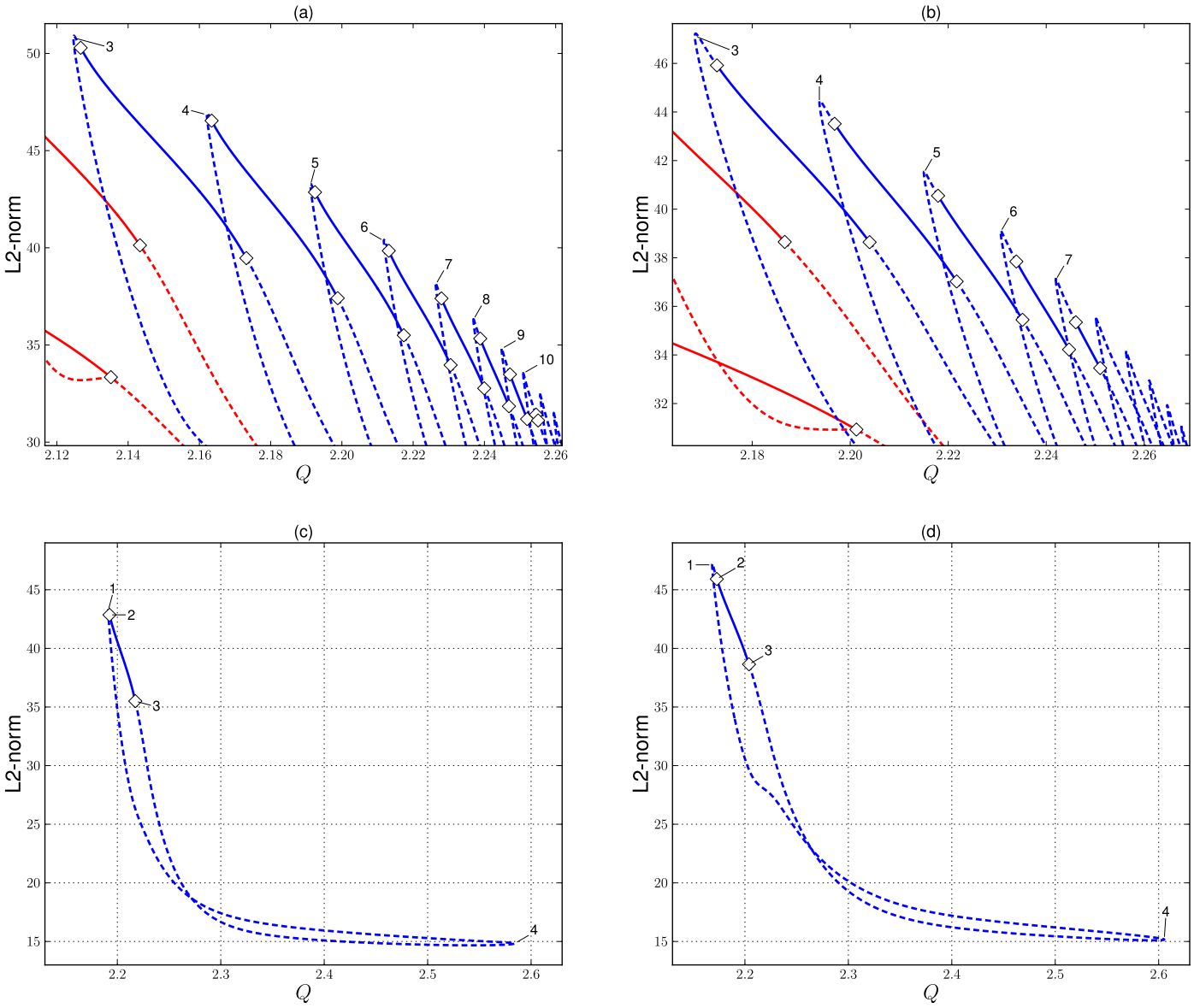

Fig. 6. Details of Fig. 5. Panel (a), for the CM, and panel (b). for the RM, show the stable Q-intervals and period-doubling bifurcations (open diamonds) near the left-hand fold of the isolas. The isolas $\mathcal{I}_n$ having a region of stability between period-doubling bifurcations are labeled ($n = 3, 4, 5, 6, \ \cdots$). Panel (c), for the CM, and panel (d), for the RM, show the isola $\mathcal{I}_3$, for which the periodic PQS self-pulsations are stable between the period-doubling bifurcations labeled 2 and 3. The folds that delimit $\mathcal{I}_3$ are labeled 1 and 4.

To the left of the *CW* near $Q = 2.25518$ in Fig. 2a, the CM shows a qualitatively different sequential behavior from that of the RM shown in Fig. 2b; a difference that can be remedied, as seen in the next section. There remain a few points that need to be mentioned. Firstly, the Q-intervals of stability for the periodic orbits $\Pi^{(n)}$ exist up to $n = 10$, as shown in Fig. 5a. As for the RM, the last Q-interval of stability exists for $n = 7$. Secondly, our numerical simulations suggest that the basin of attraction of $\Pi^{(n)}$ becomes smaller as n increases. As a result, more coexisting basins of attractors, chaotic or periodic, come into play in a small Q-interval. Thirdly, from each PD bifurcation that bounds the Q-intervals of stability of the isolas $\mathcal{I}_n$, new branches of PD solutions arise. These have in turn further Q-intervals of stability bounded by secondary PD bifurcations. This process may repeat *ad infinitum* and generates new attractors, whose

basins of attraction, however, was found to be negligibly small. Finally, extremely small regions of stability along the isolas $\mathcal{I}_n$ may also occur near the folds in Fig. 5a and Fig. 5b. The aforementioned features may induce additional chaotic attractor crises. A behavior similar to that in Fig. 2 is observed when we increase the external incoherent pump parameter Q.

As seen in both models, for higher n the stability regions along the isolas tend to shrink and disappear beyond a limiting value of n. In the next section, we show how this depends on the value of α.

5. The Stark Effect.

Here we consider briefly the changes induced by the action of an external static electrical field upon the cell of absorbing molecules in the LSA, namely, the Stark effect. A major problem in experiments with LSA concerns the relative lack of stability of the carrier frequency ("jitter") in the periodic PQS self-pulsations of $\Pi^{(n)}$. To overcome this problem, frequency locking has been induced by the Stark effect, where a periodically modulated external electrical field acts upon the absorber cell [Dangoisse *et al.*, 1990; Tsukamoto *et al.*, 1995]. An intracavity cell containing a CH_3I saturable absorber has been considered in an experiment [Dangoisse *et al.*, 1990], where it was shown that the Stark effect induces a modulation of the number of absorbing molecules. Therefore, in the equations for the CM and the RM, the parameter α depends on the voltage of the external electrical field as follows:

$$\alpha = \frac{B_a l_a N_a^*(V)}{B_g l_g} \ , \qquad N_a^*(V) = N_a^*(0)(1 + \theta V) \ ,$$

where $N_a^*(0)$ is the number of absorbing molecules at zero external voltage, $V = 0$, and θ is a suitable constant.

We assume that the Stark effect is induced by a constant (DC) electrical field, and we consider the changes in the PD bifurcations that border the Q-intervals of stability of the periodic PQS self-pulsations $\Pi^{(n)}$ as a function of Q and α. Fig. 7a and Fig. 7b show the loci of period-doublings for the CM and the RM, respectively, as the parameters Q and α change. These figures suggest that both models share the same features. In particular, we see that the Q-intervals of stability of $\mathcal{I}_n$ shrink as α decreases. Also, as α increases, new Q-intervals of stability of $\mathcal{I}_n$ appear for higher values of n. Furthermore, the first intersection between the Q-intervals of stability corresponding to the isolas $\mathcal{I}_n$ and $\mathcal{I}_{n+1}$ occurs for a value of Q smaller than that where the Q-interval of stability of $\mathcal{I}_{n+2}$ is born.

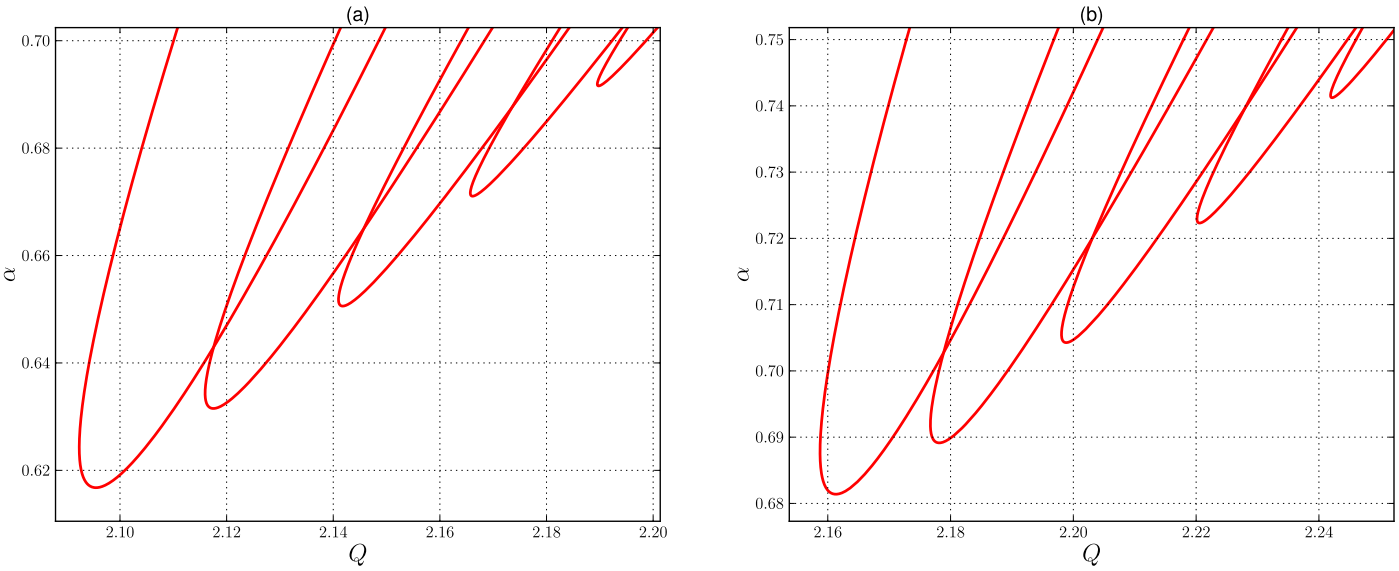

Fig. 7. Some loci of period-doubling bifurcations. The lobe-like curves correspond, from left to right, to period-doubling bifurcations along the isolas $\mathcal{I}_3, \mathcal{I}_4, \cdots \mathcal{I}_n$ (all colored red). Solutions along a given isola are stable for values of Q and α that lie inside the corresponding lobe. Panel (a) is for the CM, and panel (b) is for the RM.

The features described above indicate that a suitable, small increase of the parameter α in the RM improves the agreement of the models. Specifically, the qualitative sequence of the hysteresis effects and CW becomes more similar for increasing and decreasing Q. For example, Fig. 8a and Fig. 8b suggest that for decreasing Q the sequence $CW \rightarrow \Pi^{(5)} \rightarrow CW \rightarrow \Pi^{(4)} \rightarrow \Pi^{(3)}$ is followed, with $\alpha = 0.655$ in the CM and $\alpha = 0.71$ in the RM. For both models, CW are observed in Fig. 8a and Fig. 8b, in windows given approximately by $2.1475 < Q < 2.1687$ in the CM and $2.2065 < Q < 2.2275$ in the RM. Here there are no Q-intervals of stability for $\mathcal{I}_n$ and several unstable $\Pi^{(n)}$ already exist, as seen in Fig. 7a and Fig. 7b. In smaller CW, given approximately by $2.1379 < Q < 2.1409$ in the CM and $2.1955 < Q < 2.200$ in the RM, there is a gap with no common Q-interval of stability for $\mathcal{I}_5$ and $\mathcal{I}_4$ in both models: the two Q-intervals of stability for these isolas do not yet intersect because α is not large enough. All PQS periodic orbits $\Pi^{(n)}$ $(n > 5)$ are also unstable here. These CW are clearly observed in the simulations depicted in Fig. 8a and Fig. 8b for the CM and the RM, respectively. Fig. 7a and Fig. 7b support these observations. Thus both models, for suitable values of α, may accurately describe an experiment that observes period-adding cascades. However, the corresponding values of Q for related events in the two models are slightly different.

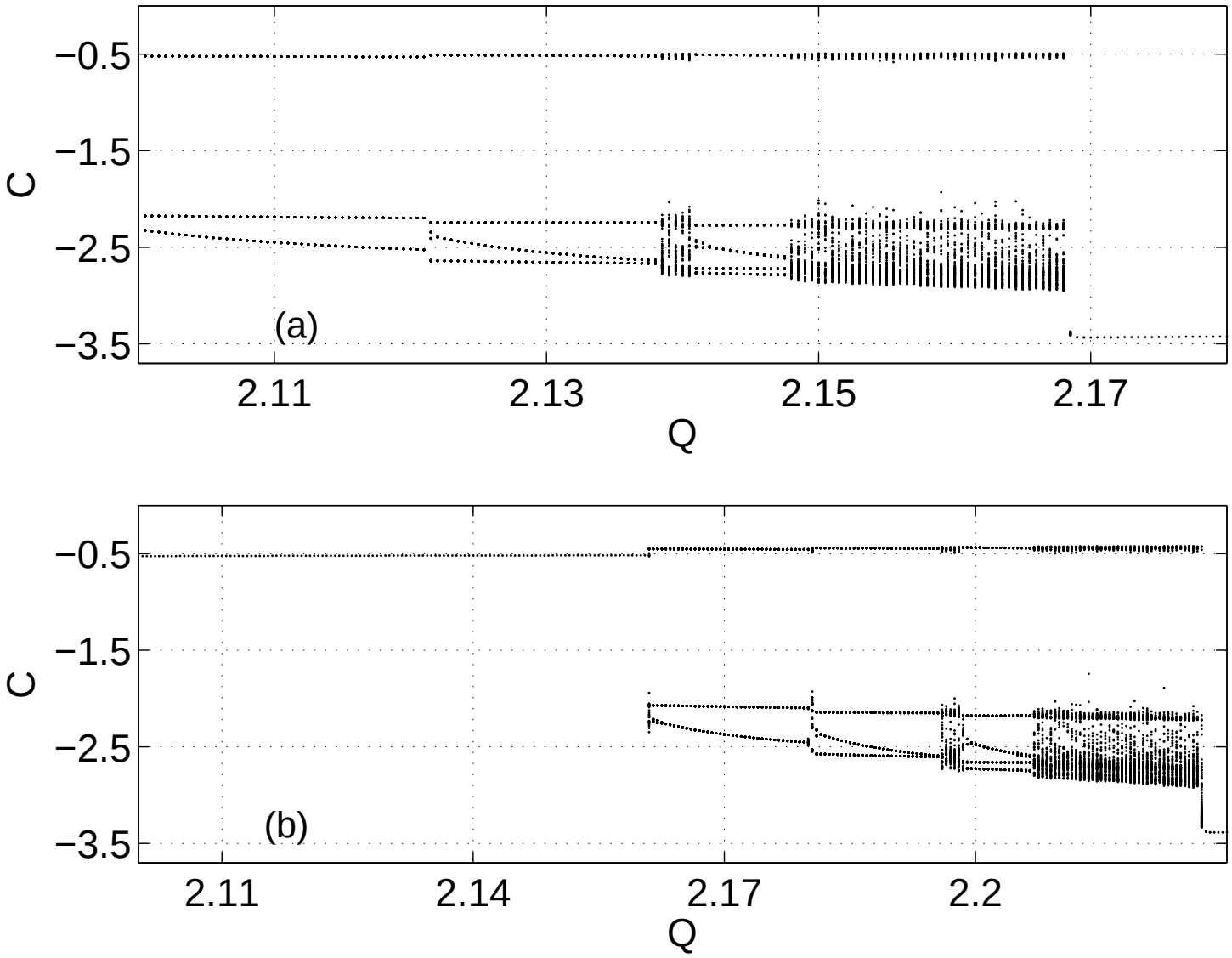

Fig. 8. Plot of c versus Q taken from the Poincaré section, where $\beta_r = 200$ and Q is being decreased. We see the period-adding cascades of periodic PQS pulses $\Pi^{(n)}$, and windows of chaotic behavior. Panel (a) is for the CM, where $\alpha = 0.655$, and panel (b) is for the RM, where $\alpha = 0.71$.

Finally we point out that the Stark effect also induces changes in the isolas $\mathcal{I}_n$. Indeed, this can be seen in Fig. 9a and Fig. 9b for the CM and the RM, respectively. As a measure of the size of the isolas $\mathcal{I}_n$, it is natural to consider the location of their folds. One can see that the rightmost folds are found at basically the same value of Q for all isolas with a given value of α. In contrast, the leftmost folds are at different locations, but approach each other for large n.

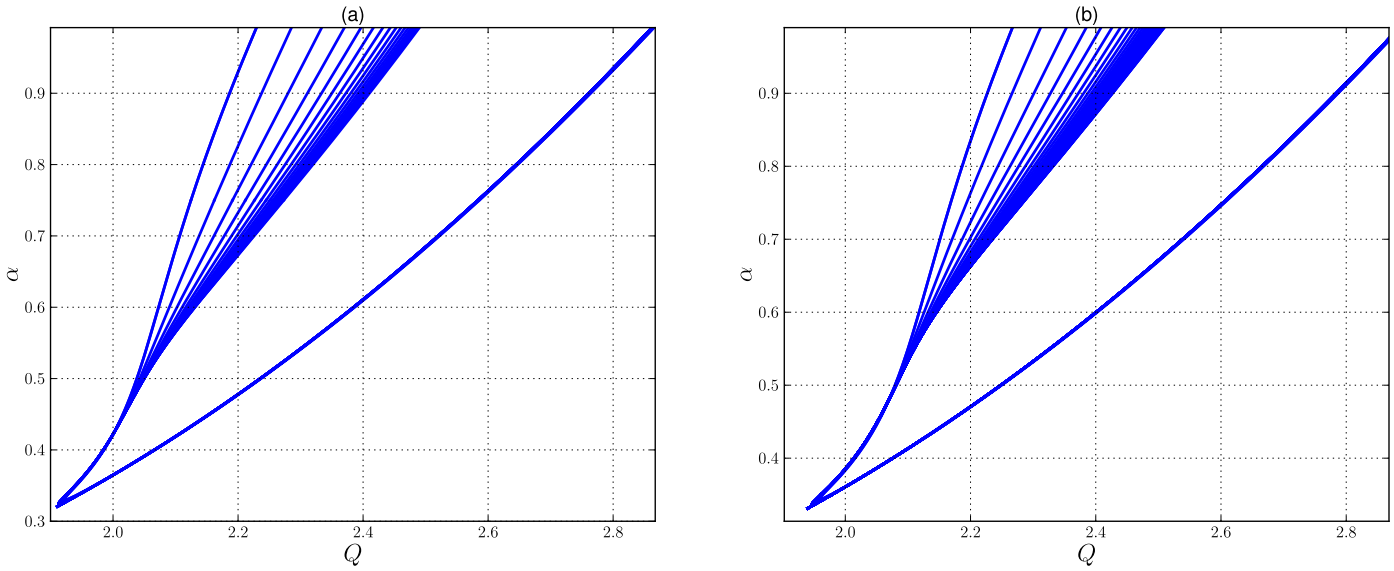

Fig. 9. The loci of folds of isolas $\mathcal{I}_n, n = 3, 4, 5, \cdots$. Panel (a) is for the CM, and panel (b) is for the RM. Note that, for example for $\alpha = 0.6$, all isolas are delimited on the right near the value $Q = 2.4$, while on the left they are delimited by quite distinct values of Q, as also seen in Figures 5 and 6. In this figure $\beta_r = 200$.

In both models the mechanism by which the isolas disappear is via the well-known "isola formation points", *i.e.*, the points at the lower limits of the loci of folds in Fig. 9a and Fig. 9b. However, as seen in the detail shown in Fig. 10a and Fig. 10b, the situation is somewhat more complicated. What happens is that the isola first breaks into two separate isolas, which then disappear one after the other, as suggested by these figures. The later indicates that the nature of the origin of the isolas in both models is the same.

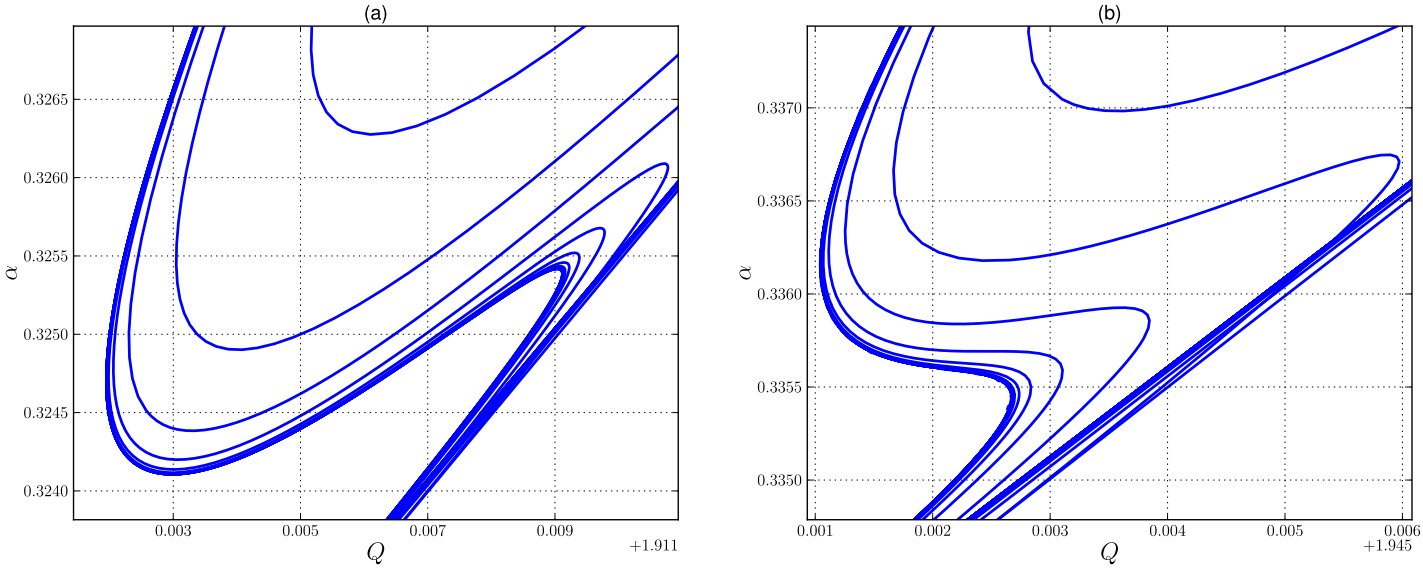

Fig. 10. A further detail of Fig. 9 showing the loci of folds of isolas $\mathcal{I}_n$. Panel (a) is for the CM, and panel (b) is for the RM. Along the horizontal axis the Q-value is the sum of the value marked along the axis and the nominal value located at the bottom right of the panel. In this figure $\beta_r = 200$.

6. Conclusions and Discussion

We have presented a systematic comparison of a molecular model of a CO_2 laser with a fast saturable absorber and a reduced version of this model. Qualitatively the agreement of the bifurcation structure of the complete model (CM) and the reduced model (RM) is found to be very good. At the quantitative level there are some differences, which manifest themselves in the numerical simulation of the hysteresis behavior between different attractors, as the incoherent pump parameter Q is changed.

The first new relevant feature explored in this article is the description of the hysteresis dependence on codimension-1 and codimension-2 bifurcations in both the complete model (CM) and the reduced model (RM). Indeed, Fig. 6, Fig. 7 and Fig. 10 show how to obtain a good qualitative agreement of both models, as we sweep the parameter Q, as shown in Fig. 8. These figures show how the bifurcations move in parameter space as a result of the reduction. A practical conclusion is that the bifurcations in parameter space (Q, α) show that a small increase of the secondary parameter α in the RM with respect to that of the CM substantially improves the quantitative agreement of the models.

The second relevant feature, assuming a fixed value for α, is that the Q-intervals of stability of $\Pi^{(n)}$ along isola $\mathcal{I}_n$ may show either a region or regions of intersection of such stability intervals of the neighboring isolas $\mathcal{I}_n$ and $\mathcal{I}_{n+1}$ or a region that separates these stability intervals. In the former case, the region or regions of intersection is where coexistence of two or more $\Pi^{(n)}$ occurs. Instead, in the latter case, the aforementioned region is where chaotic behavior can take place. The behavior in this interval depends ultimately on the existence of unstable $\Pi^{(n)}$ and other possible attractors. The latter is supported by simulations where the parameter Q is changed. As a result, the bounds of the chaotic windows are located in a very close neighborhood of period-doubling bifurcations, which in turn determine the Q-intervals of stability of $\mathcal{I}_n$. Indeed, Fig. 7 indicates that as we sweep the parameter Q, typically at most two chaotic windows can occur for both the CM and the RM, where the unstable $\Pi^{(n)}$ can trigger the chaotic dynamics in this interval.

Lack of a comprehensive study of the relationship of the bifurcations in CM and RM has led in recent years to the almost exclusive use of the CM either for the amplifier or absorber, underestimating or disregaring the usefulness of the RM. This applies in particular to several CO2 laser models. The present article shows how a mapping of parameters of the CM and the RM can be carried out to recover essentially the same dynamics.

In our previous article [Doedel *et al.*, 2011a], we found that periodic passive Q-switching self-pulsations having the same number of undulations belong to isolas of periodic orbits with changing incoherent pump parameter Q. In both models the physically relevant Q-intervals, where the PQS periodic self-pulsations are stable along a given isola, are bordered by period-doubling bifurcations. The coexistence of such stability intervals induces the observed experimental phenomenon known as period-adding cascades.

We believe that it is of interest to implement control techniques in nonlinear dynamics [Boccaletti *et al.*, 2000; Sieber *et al.*, 2008], in the context of an experiment as well as in the present models. Indeed, using the changes induced by the Stark effect, when a DC electrical field acts upon the absorber cell, and changes in the incoherent pump parameter, it seems possible to determine experimentally the existence of isolas and their Q-intervals of stability. In this context, we think that an interesting problem is the study of the nature of complex networks of self-similar stability islands in the presence of isolas of periodic orbits, as in our models. In particular, these complex networks have been studied in the context of the Hénon map [Gallas, 1993] and a loss-modulated class-B laser model [Bonatto *et al.*, 2005].

Finally, we mention two perspectives within the scope of nonlinear dynamics for the CO_2 LSA. The first one points to the need for a more quantititative correspondence between the experiments and the model, as indicated by Cavalcante and Rios-Leite [Cavalcante & Rios Leite, 2008]. These authors refer to the relation between suitable maps, as discussed by Gaspard and Wang [Gaspard *et al.*, 1987], and the homoclinic features observed in the experiment. We believe that a study of higher-codimension bifurcations, with Q, α and β_r as parameters, will give additional insight compared to those predictions based on maps [Gaspard *et al.*, 1987]. In particular, we refer to the widths of the experimental periodic windows: the parameter β_r does not have a straightforward analog in the map of Gaspard and Wang [Gaspard *et al.*, 1987]. The second perspective concerns the issue of excitability. Indeed, in an article of Plaza and collaborators [Plaza

et al., 1997], an experiment shows a new excitability scenario in the CO_2 LSA. We believe that our reduced model is a good starting point to study this kind of dynamics. Finally we note that excitable laser systems have received significant attention in recent years [Kelleher *et al.*, 2011].

Acknowledgments

This work was supported by NSERC (Canada), the Instituto de Física, Benemérita Universidad Autónoma de Puebla, CONACYT (México), and the VIEP programme.

References

Abraham, N. B., Mandel P. & Narducci L. M. [1998] "Dynamical instabilities and pulsations in lasers," in *Progress in Optics XXV*, ed. Wolf, E. (North-Holland), pp. 3–190.

Arecchi, F. T. [1987] "Instabilities and chaos in single-mode homogeneous line lasers" in *Instabilities and Chaos in Quantum Optics*, eds. Arecchi, F. T. & Harrison, R. G. (Springer), pp. 9–48.

Arimondo E., Casagrande F., Lugiato L. & Glorieux P. [1983] "Repetitive passive Q-switching and bistability in lasers with saturable absorbers," *Appl. Phys. B: Photophys. Laser Chem.* **30**, 57–77.

Boccaletti, S., Grebogi, C., Lai, Y. C., Mancini, H. & Maza, D. [2000] "The control of chaos: theory and applications," *Physics Reports* **329**, 103–197.

Bonatto, C., Garreau, J. C. & Gallas, J. A. C. [2005] "Self-Similarities in the Frequency-Amplitude Space of a Loss-Modulated CO2 Laser," *Phys. Rev. Lett.* **95**, 143905.

Braza, P. [1999] Poster session at the *Fifth SIAM Conference on Applications of Dynamical Systems*, May 23–27, Snowbird, Utah, USA.

Brons, M., Kaper, T. J. & Rotstein H. G. [2008] "Introduction to Focus Issue: Mixed Mode Oscillations: Experiment, Computation, and Analysis," *Chaos* **18**, 015101.

Burak, I., Houston, P., Sutton, D. & Steinfeld, J. [1971] "Mechanism of passive switching in CO_2 lasers," *IEEE J. Quantum Electron.* **7**, 73–82.

Cavalcante, H. L. D. de S. & Rios Leite J. R. [2008] "Experimental bifurcations and homoclinic chaos in a laser with a saturable absorber," *Chaos* **18**, 023107.

Ciofini, M., Politi, A. & Meucci, R. [1993] "Effective two-dimensional model for CO_2 lasers," *Phys. Rev. A* **48**, 605–610.

Dangoisse, D., Bekkali, A., Papoff, F. & Glorieux, P. [1988] "Shilnikov dynamics in a passive Q-switching laser," *Europhys. Lett.* **6**, 335–340.

Dangoisse, D., Glorieux, P. & Hennequin, D. [1990] "Nonlinear dynamics of a laser containing a modulated saturable absorber," *Phys. Rev. A* **42**, 1551–1559.

Doedel, E.J. [1984] "Continuation techniques in the study of chemical reaction schemes,", in: *Proc. Special Year in Energy Math., Univ. of Wyoming, K. I. Gross, ed., SIAM Publ.*, 103–138

Doedel, E. J., Oldeman, B. E. *et al.* [2011] "AUTO-07P: Continuation and bifurcation software for ordinary differential equations,", Version 0.8, Concordia University, Montréal, Canada.

Doedel, E. J., Oldeman, B. E. & Pando L., C. L. [2011] "Bifurcation structures in a model of a CO_2 laser with a fast saturable absorber," *International Journal of Bifurcations and Chaos* **21**, 305–322.

E.J. Doedel & C.L. Pando L. [2011], "Isolas of Periodic Passive Q-switching Self-Pulsations in the 3-2 Level Model for a Laser with a Saturable Absorber," accepted for publication, 2011.

Dupré, J., Meyer, F. & Meyer, C. [1975] "Influence des phénomènes de relaxation sur la forme des impulsions fournies par un laser CO_2 déclenché par un absorbant saturable," *Rev. Phys. Appl. (Paris)* **10**, 285–293.

Erneux, T. & Glorieux, P. [2010] *Laser Dynamics* (Cambridge University Press, New York).

Gallas, J. A. C. [1993] "Structure of the parameter space of the Hénon map," *Phys. Rev. Lett.* **70**, 2714–2717.

Gaspard, P. & Wang X. J. [1987] "Homoclinic orbits and mixed-mode oscillations in far-from-equilibrium systems," *Journal of Statistical Physics* **48**, 151–199.

Hennequin, D., de Tomasi, F., Zambon, B. & Arimondo, E. [1988] "Homoclinic orbits and cycles in the instabilities of a laser with a saturable absorber," *Phys. Rev. A* **37**, 2243–2246.

Horbelt, W., Timmer, J., *et al.* [2001] "Identifying physical properties of a CO_2 laser by dynamical modeling of measured time series," *Phys. Rev. E* **64**, 016222.

Kantz, H. & Schreiber, T. [2004] *Nonlinear Time Series Analysis* (Cambridge University Press, New York).

Kelleher, B., Bonatto, C. *et al.* [2011] "Excitability in optically injected semiconductor lasers: Contrasting quantum-well- and quantum-dot-based devices," *Phys. Rev. E* **83**, 026207.

Keller, U. [2003] "Recent developments in compact ultrafast lasers," *Nature* **424**, 831-838.

Kuznetsov, Y. [2004] *Elements of Applied Bifurcation Theory* (Springer-Verlag, New York).

Lefranc, M., Hennequin, D. & Dangoisse, D. [1991] "Homoclinic chaos in a laser containing a saturable

absorber," *J. Opt. Soc. Am. B* **8**, 239–249.

Mandel, P. [1997] *Theoretical Problems in Cavity Nonlinear Optics* (Cambridge University Press, New York).

Marino, I. P., Allaria, E. *et al.* [2003] "Information encoding in homoclinic chaotic systems" *Chaos* **13**, 286-290.

Meucci, R., Ciofini, M. & Wang, P. Y. [1992] "Analysis of the dynamical behavior of a Q-switched CO_2 laser: the linear and the nonlinear regime," *Optics Comm.* **91**, 444–452.

Olsen, R.J. & Vlachos D.G. [1999] "A Complete Pressure-Temperature Diagram for Air Oxidation of Hydrogen in a Continuous-Flow Stirred Tank Reactor," *J. Phys. Chem. A* **103**, 7990–7999.

Papoff, F., Fioretti, A., Arimondo, E., Mindlin G.B., Solari, H. & Gilmore, R. [1992] "Structure of chaos in the laser with saturable absorber," *Phys. Rev. Lett.* **68**, 1128–1131.

Pando L., C. L., Meucci, R., Ciofini, M. & Arecchi, F. T. [1993] "CO_2 laser with modulated losses: Theoretical models and experiments in the chaotic regime," *Chaos* **3**, 279–285.

Pando L., C. L., Luna A., G. A., Meucci, R. & Ciofini, M. [1995] "Highly dissipative Hénon map behavior in the four-level model of the CO_2 laser with modulated losses," *Phys. Lett. A* **199**, 191–198.

Pando L., C. L. [1996] "Recurrent synchronism in the internal dynamics of CO_2 lasers," *Phys. Lett. A* **210**, 391–401.

Plaza F., Velarde, M. G., Arecchi F. T., Boccaletti, S.,Ciofini, M., & Meucci, R. [1997] "Excitability following an avalanche-collapse process," *Europhysics Letters* **38**, 85–90.

Sieber, J., Gonzalez-Buelga, A., Neild, S. A., Wagg, D. J. & Krauskopf, B. [2008] "Experimental continuation of periodic orbits through a fold," *Phys. Rev. Lett.* **100**, 244101.

Siegman, E. [1986] *Lasers* (University Science Books).

Tachikawa, M., Tanii, K., Kajita, M & Shimizu, T. [1986] "Undamped Undulation Superposed on the Passive Q-Switching Pulse of a CO_2 Laser," *Appl. Phys. B: Photophys. Laser Chem.* **39**, 83–90.

Tachikawa, M., Tanii, K. & Shimizu, T. [1987] "Comprehensive interpretation of passive Q switching and optical bistability in CO_2 laser with an intracavity saturable absorber," *J. Opt. Soc. Am. B* **4**, 387–395.

Tachikawa, M., Hong, F. L., Tanii, K. & Shimizu, T. [1988a] "Deterministic chaos in passive Q-switching pulsation of a CO_2 laser with saturable absorber," *Phys. Rev. Lett.* **60**, 2266–2268.

Tohei, T., Tachikawa, M., & Shimizu, T. [1992] "Rate-equation analysis of deterministic chaos in a laser with a saturable absorber," *Phys. Rev. A* **45**, 5166–5170.

Tsukamoto, T., Tachikawa, M., Sugawara, T. & Shimizu, T. [1995] "Locking of a passive Q-switched chaotic laser system to a small external modulation," *Phys. Rev. A* **52**, 1561–1569.

Varone, A., Politi, A. & Ciofini, M. [1995] "CO_2 laser dynamics with feedback," *Phys. Rev. A* **52**, 3176–3182.

Wang, T. J., He, Q. Y. *et al.* [2006] "Comparison between four-level model and six-temperature model on the description of a simple mechanical Q-switched CO_2 laser," *Journal of Applied Physics* **100**, 023121.

Wood, O.R. & Shwarz, S.E. [1967] "Passive Q-switching of a CO_2 laser," *Applied Physics Letters* **11**, 88–89.

Zambon, B., de Tomasi, F., Hennequin, D. & Arimondo, E. [1989] "Investigations of models and experimental studies of a stationary regime for a laser with a saturable absorber," *Phys. Rev. A* **40**, 3782–3795.

Zambon, B. [1991] "Theoretical investigations of models for the laser with a saturable absorber: A case of homoclinic tangency to a periodic orbit," *Phys. Rev. A* **44**, 688–702.

Zehnle, V., Dangoisse, D. & Glorieux, P. [1992] "Behavior of a CO_2 laser under loss modulation: critical analysis of different theoretical models," *Optics Comm.* **90**, 99–105.